V. RADIO ASTRONOMY*

Academic and Research Staff

Prof. A. H. Barrett
Prof. B. F. Burke
Prof. R. M. Price
Prof. D. H. Staelin
Dr. G. D. Papadopoulos
J. W. Barrett
D. C. Papa

Graduate Students

R. H. Cohen
P. C. Crane
M. S. Ewing
T. D. Halket
H. F. Hinteregger
P. L. Kebabian
C. A. Knight
K-S. Lam
K-Y. Lo
P. C. Myers
P. W. Rosenkranz
P. R. Schwartz
J. H. Spencer
J. W. Waters
A. R. Whitney

RESEARCH OBJECTIVES AND SUMMARY OF RESEARCH

The program in radio astronomy comprises very long baseline interferometry, in which highly stable atomic frequency standards are used to control frequency and time to permit the operation of radio interferometry over arbitrarily long baselines; radio spectroscopy of the interstellar medium, specifically studies of OH, H_2O and H II emission and absorption; study of pulsars; and the use of radio astronomical techniques to study the Earth's atmosphere.

1. Aperture Synthesis

A 2-cm interferometer has been completed and the working system has been used to demonstrate that the phase stability of the atmosphere is sufficient to allow interferometry at shorter wavelengths. The instrument serves as a prototype for an aperture synthesis interferometer using larger elements. These elements, 18' in diameter, are now being ordered and construction of the new instrument will begin in early 1971.

2. Very Long Baseline Interferometry of H_2O Sources

The extension of VLBI techniques to higher frequencies resulted in the successful operation of an experiment to measure the source sizes and distribution of celestial H_2O sources. The wavelength, 1.34 cm, is the shortest wavelength at which the technique has been successfully used, and the resolution achieved between the Haystack Observatory and the NRAO 36' telescope at Kitt Peak gives a resolution of .0006 seconds of arc, the highest angular resolution ever achieved. The technique is being perfected and extended to other sources and we expect to observe quasi-stellar sources in addition to H_2O line emitters.

---

*This work was supported principally by the National Aeronautics and Space Administration (Grants NGL 22-009-016 and NGL 22-009-421) and the National Science Foundation (Grants GP-20769 and GP-21348), and in part by the Joint Services Electronics Programs (U.S. Army, U.S. Navy, and U.S. Air Force) under Contract DA 28-043-AMC-02536(E), California Institute of Technology Contract 952568, and the Sloan Fund for Basic Research (M.I.T. Grant 241).

3. Application of VLBI Techniques to Geodesy and Navigation

An observing program has been continuing to demonstrate the feasibility of making distance measurements over the surface of the earth with much greater accuracy than achievable by other methods. An experiment has been completed in which the distance between the Haystack telescope and the 140' telescope in Green Bank, West Virginia, has been determined with an accuracy of ±4 meters over a baseline 845 km long. The observations are continuing with a view to improving the accuracy and demonstrating the repeatability of the technique.

4. Microwave Spectroscopy of the Interstellar Medium

The H_2O line emission from Mira-type variable stars has been shown to vary in phase with the light variation. OH emission from highly excited rotational states of OH was discovered in a number of sources, and searches for other microwave lines of OH, its various isotopic species, and other molecules are continuing.

5. Pulsar Antenna

A very simple antenna, equivalent in aperture to a 200' dish, has been constructed to observe pulsars at frequencies of 300 MHz and lower. The equipment has been completed and a program of observation and testing will continue through 1971.

6. Pulsar Spectrometry

Multichannel receiver spectrometry of pulsars continues, in an effort to relate the observed regularities, both short term and long term, with theories of propagation of electromagnetic waves in inhomogeneous media.

7. Radio Astronomy Studies of the Earth's Atmosphere

The program of balloon-based atmospheric observations continues. In addition, ground-based studies of the upper atmospheric ozone, H_2O, and oxygen have been carried out to determine water vapor content and temperature structure of the meso- and stratosphere. An aircraft-borne radiometer has been tested, preliminary to the satellite-borne oxygen and water observations to be conducted in the Nimbus series.

A. H. Barrett, B. F. Burke

A. SEARCH FOR THE $2^2P_{3/2} - 2^2S_{1/2}$ LINE OF INTERSTELLAR HYDROGEN

The role played by neutral hydrogen and helium atoms in HII regions has been studied primarily by observing radio-frequency spectral lines from highly excited (principal quantum $n \sim 100$) atoms (recombination lines) and optical lines from atoms of lower excitation ($n < 5$). We shall report a search for 3-cm radiation from the $2P_{3/2}$-$2S_{1/2}$ transition of atomic hydrogen in several galactic HII regions. In all cases no line stronger than a sensitivity limit of $0.2°K = 3\Delta T_{rms}$ was detected.

1. Observations

The observations were made during April 1970 with the 37-m antenna of the Haystack Observatory of Lincoln Laboratory, M.I.T.* The beam-switched superheterodyne radiometer had a 1-GHz bandwidth and a system temperature of approximately 1000°K.

The comparison horn was a wide-beam standard-gain horn elevated at 45° with respect to the main horn. After amplification by a tunnel diode amplifier, the 1-GHz RF band centered at 9.9 GHz was mixed with either 11.4 GHz (L.O. 1) or 11.3 GHz (L.O. 2) to produce an IF band from 1.0 GHz to 2.0 GHz. This band was then divided into 8 channels. The voltage in each channel was then filtered, square-law detected, amplified, synchronously demodulated, converted to a digital signal, and fed into a Univac 490 computer which wrote the digital signals on magnetic tape. Calibration for all channels was provided by an argon gas tube, attenuated to provide a 10°K noise input into the signal arm of the radiometer.

The local-oscillator and filtering scheme was designed to place 16 channels, each 10 MHz wide, across the 1-GHz band so that the maximum useful information about the spectral line could be obtained. The unusually large linewidth (>300 MHz) necessitated an observing bandwidth (1 GHz) large enough to provide several points on either side of the line, so that the baseline could be determined accurately. Since the expected spectral line is actually a blend of 3 hyperfine components, a second design consideration was placement of a filter at the center frequency of each hyperfine component. A third consideration was closer spacing of on-line filters than off-line. The filtering scheme that was finally adopted is shown in Fig. V-1. The two klystrons were kept running continuously to avoid warm-up drift; each was isolated and attenuated to provide the proper output level. The local-oscillator frequency to be used as the mixer input was selected by means of a remotely operated coaxial switch. On the average, the switch was thrown once every 4 or 5 observing hours.

In the course of the observations we noticed two instrumental contributions to the spectra. The first is an elevation dependence on the antenna temperature, that is, to the difference between the temperatures of the main horn and the comparison horn. We believe that this decrease in temperature with elevation is due principally to ground radiation preferentially entering the main horn, directly or after scattering by the metal radome skeleton at low antenna elevation angles. The second effect is a nonlinear baseline slope, higher at the low-frequency end of the spectrum; the difference between highest and lowest temperatures was typically as much as 40% of the mean. After tests of the radiometer components, we concluded that the spectral properties of the noise tube and feed horns, and their interaction with the ferrite switch, were

*Lincoln Laboratory is operated by M.I.T. with the support of the U.S. Air Force.

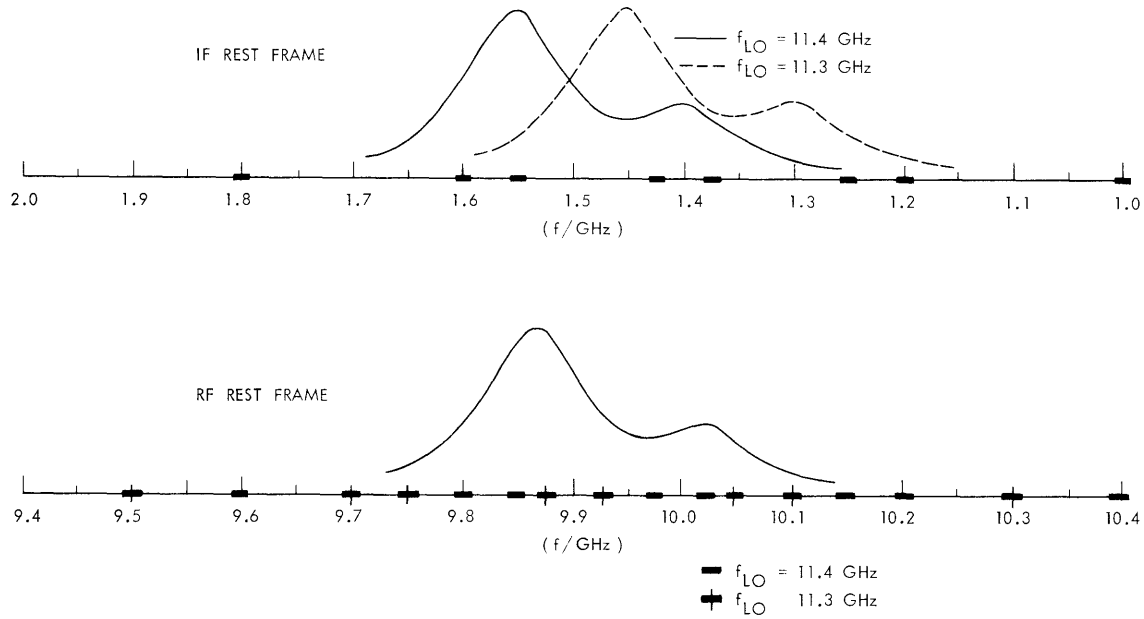

Fig. V-1. Eight-channel filtering scheme.

the chief contributors to the baseline slope. The reproducibility of both of these effects was determined in advance by repeated observations of Cas A at various elevations. This reproducibility was good enough to enable us to adopt the observing and data-processing procedures described below.

For each local-oscillator setting and source, we performed a sequence of runs: an off-source run, usually 10 min long, during which the main antenna beam was offset by 1° in azimuth from the source position; a 5-min calibration run with the same offset and with the 10°K noise signal injected into the radiometer signal arm; and a 10-min on-source run. For each source, we spent equal times observing with L.O. 1 and L.O. 2, in order to obtain comparable sensitivity for both octets of frequency channels. For each H II region that we observed, we also observed a nonthermal source at a nearby elevation, according to the sequence just described. These "calibration" sources produced spectra whose slope is very similar to that of the H II region spectra. Yet we are quite certain that they do not contain the line, because of their low neutral hydrogen content and the coldness of the neutral hydrogen along the intervening line of sight. Thus, the difference between the H II region spectrum and the corresponding calibration spectrum, appropriately scaled, should remove the sloping baseline and leave the true spectrum, if the baseline is instrumental. The surprisingly high sensitivity and frequency flatness of the different spectra that we found confirm our initial belief that the baseline is instrumental, repeatable, and separable.

The data processing was performed at Haystack on the CDC 3300 computer. It was divided into two parts, each performed by a separate Fortran program. The first

program reads the magnetic data tape written by the Univac 490 computer, extracts for each 30-sec scan the 8 integrated channel voltages, the source elevation, the time, and the identification number, into which are encoded the source, local-oscillator numbers, and run type (off-source, calibration or on-source). It then translates these quantities from 30-bit into 24-bit words, and stores them in arrays. For each source, L.O., run type and channel, it computes the mean and standard deviation of all scan voltages in a run, and writes these, together with the appropriate timing, elevation, and coding information, on an output tape. After this first program is used to process all data tapes (more than 20 altogether), the resulting output tape is used as the input to the second program.

The second program computes antenna temperatures and plots source spectra. It learns which source and calibration are to be used from a card input. It then searches the tape for records containing relevant information and reads them into storage. It computes the antenna temperature for each source, L.O. channel and run, according to the formula

$$T_{Ai} = 10\left(\frac{\overline{V}_i\,(\text{on-source}) - \overline{V}_i\,(\text{off-source})}{\overline{V}_i\,(\text{calibration}) - \overline{V}_i\,(\text{off-source})}\right), \qquad i = 1, \ldots 8$$

It then groups these 8-point temperature spectra into pairs, selecting for each source run a calibrator run whose initial elevation is nearest the initial elevation of the source run. A scaling factor ρ is computed, according to the formula

$$\rho\,(\text{source, L.O., run}) = \frac{1}{6}\left(\sum_{i=1}^{3} T_i\,(\text{source, L.O., run}) \Big/ T_i(\text{calibrator, source, L.O., run'}) + \sum_{i=6}^{8} T_i\,(\text{source, L.O., run}) \Big/ T_i\,(\text{calibrator, L.O., run'})\right).$$

Here run' is the calibrator run that is paired with the source run. Channels 4 and 5 are omitted in the computation of ρ so that it will express the mean ratio of baseline points, and will not be significantly changed by the presence of a line in the center channels. The baseline subtraction is then performed:

$$T_i^{\text{spectrum}}\,(\text{source, L.O., run}) = T_i\,(\text{source, L.O., run}) - \rho T_i\,(\text{calibrator, L.O., run'}).$$

This procedure is repeated for each run, taken for each L.O. The resultant 8-point spectra are then combined to give 16-point spectra of the lowest standard deviation. Several of these spectra are then averaged together to give the spectra displayed in Fig. V-2.

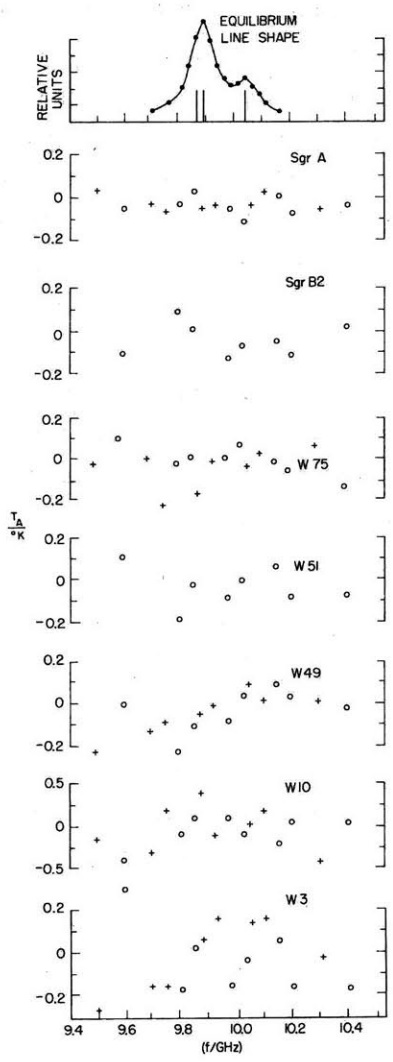

Fig. V-2. Observed source spectra. Circles represent data taken with L.O. 1 (11.4 GHz); crosses represent data taken with L.O. 2 (11.3 GHz).

2. Results of Observations

The H II regions for which we obtained 16-point spectra are listed in Table V-1, together with ΔT_{rms}, the standard deviation for each source spectrum, and T_{max}, the upper limit on the antenna temperature of the line in either absorption or emission, under the assumption $T_{max} = 3\Delta T_{rms}$. The results for the nonthermal component

Table V-1. Observational results for 16-point spectra.

Object	ΔT_{rms}	T_{max}
Sgr A	0.02° K	0.06° K
W75	0.08	0.24
W49	0.04	0.12
W10	0.23	0.69
W3	0.06	0.18

Note. Because of poor observing conditions the spectra obtained on L.O. 2 from Sgr B2 and W51 are not presented.

of the galactic center, Sgr A, are also included in Fig. V-2. The expected emission line shape for a Boltzmann distribution of hyperfine state population is given in order to provide a reference against which to compare the spectra.

We consider the experimental part of this project to be completed. A more extensive report is being prepared for publication.

A. H. Barrett, J. W. Barrett, P. C. Myers, D. C. Papa

B. EFFECTS OF CLOUDS ON INDIRECT SENSING OF ATMOSPHERIC TEMPERATURE

Computations of the perturbation in nadir brightness temperature as seen from space, caused by a model cloud of 1.5 km thickness in the U.S. Standard Atmosphere are shown in the form of contour plots in Figs. V-3, V-4, and V-5 for two of the frequencies to be used by the Nimbus-E microwave spectrometer (NEMS). The weighting functions of the two higher NEMS frequencies peak high enough so that they will not be appreciably affected by clouds. The effect at the fifth frequency, 22.2 GHz, is similar to that at 31.4 GHz. Microwave absorption by liquid water droplets was computed using the long-wavelength theory of Gunn and East,[1] which is valid to a good approximation, at the highest frequency considered here, for droplets of less than 100-μ diameter. When rain drops are present, an analytical treatment becomes more complicated

because of scattering. The temperature dependence of the dielectric constant for water is based on measurements by Collie, Ritsen, and Hasted.[2] The abscissae of the plots,

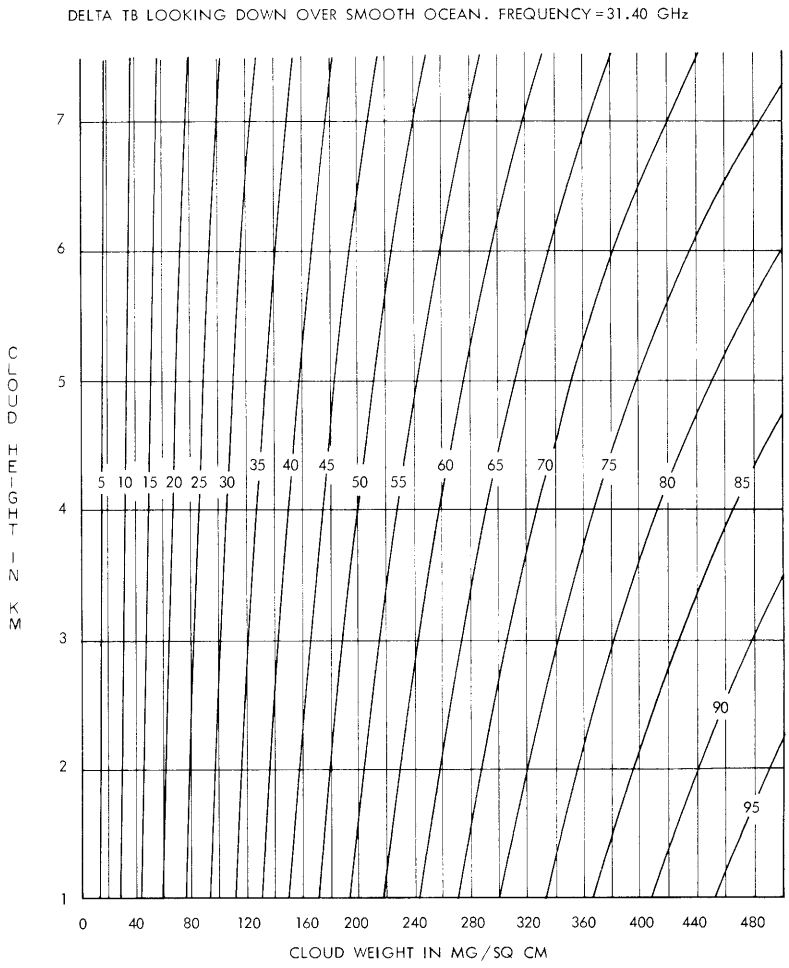

Fig. V-3. Delta TB looking down over smooth ocean. Frequency 31.40 GHz.

the height of the center of the cloud, extends only to 7 km for the reason that clouds higher than this can be expected to be in the form of ice crystals, whose interaction with microwaves is several orders of magnitude less than that of liquid water droplets. For the case of clouds of thickness different from 1.5 km, the effect on brightness temperature would be a superposition of the effects of thinner clouds of the same density, the exact characteristics of which would depend on the optical depth of the cloud; however, the general effect would be similar to the case shown here.

Figure V-6 shows inversions of radiometric data obtained on the 1970 Airborne Meteorological Expedition during overflight at 34,000 ft of a Pacific Ocean cold front.

This is the first demonstration of the ability of microwaves to measure temperature and water vapor through clouds. The points marked "infrared" were obtained

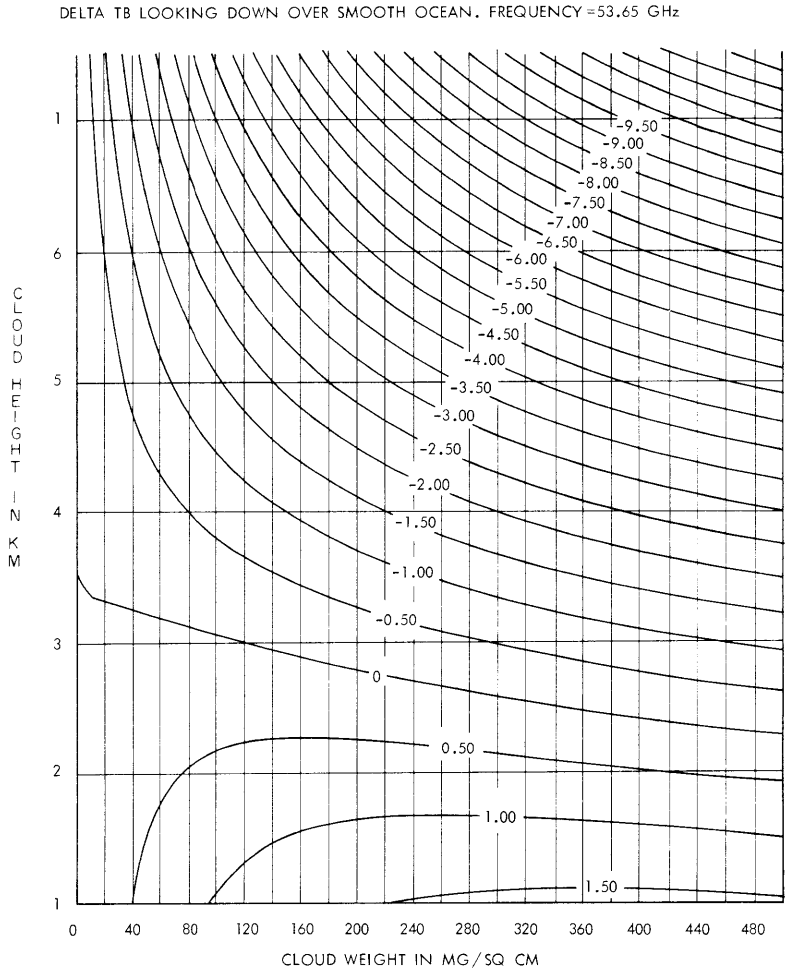

Fig. V-4. Delta TB looking down over smooth ocean. Frequency 53.65 GHz.

by a separate experiment on board the aircraft which measured local air temperature. The effect produced on the inversion by a cloud would be expected to be approximately equal to the change in brightness temperature at 53.65 GHz multiplied by the corresponding coefficient in the inversion matrix,[3] which is 0.6 for the surface temperature. Since the mean height of the multilayered cloud system associated with this front was in the 2-3 km range where the perturbation of brightness temperature at 53.65 GHz is near zero, there is no change in the estimated surface temperature over the heaviest part of the cloud.

Because of the temperature dependence of the cloud absorption coefficient, the measurement of liquid water content obtained from the 22.235 GHz and 31.4 GHz

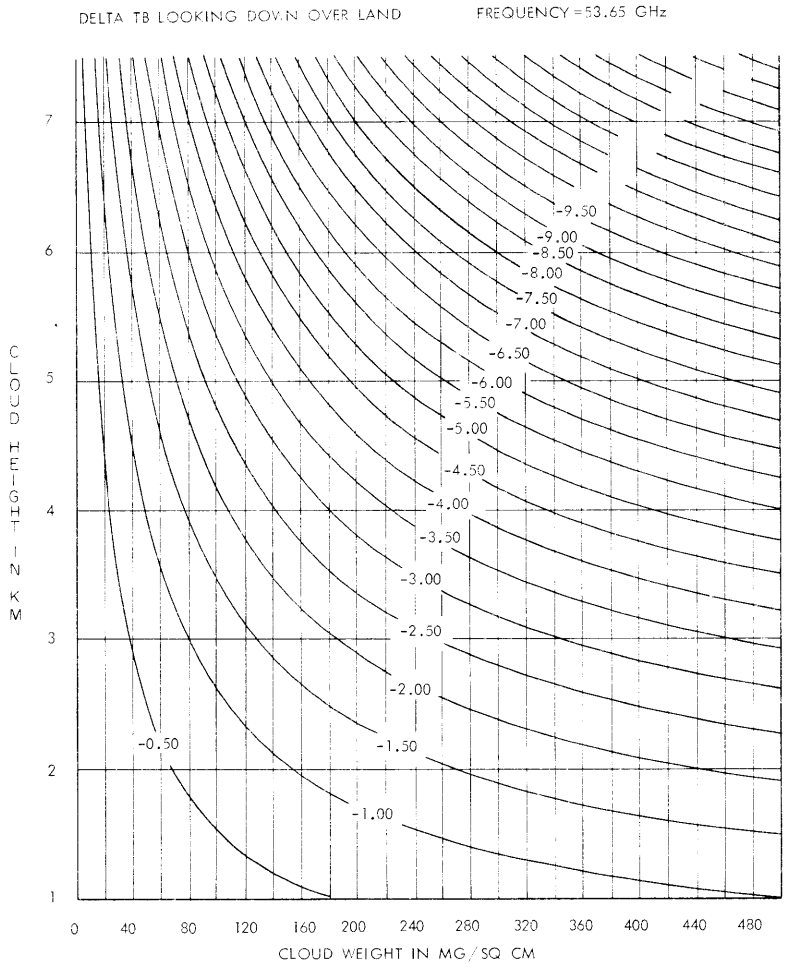

Fig. V-5. Delta TB looking down over land. Frequency 53.65 GHz.

data over water is not affected by the height (or temperature) of the cloud. The effect of the cloud at 53.65 GHz is strongly height-dependent, however, so the measurement of liquid-water content is in general not of use in inverting the data to obtain atmospheric temperature. (The height of the top of the cloud can be obtained from an infrared spectrometer, but not the mean height.) Moreover, the average height of heavy clouds will be near the range where their effect over water is small. Over land, the effect of clouds is greater, as Fig. V-4 shows, but here, because of the high and variable emissivity of the

surface, liquid-water content cannot be measured. Because NEMS will average over a large area when looking down from space, however, dense clouds of limited extent may not present a problem.

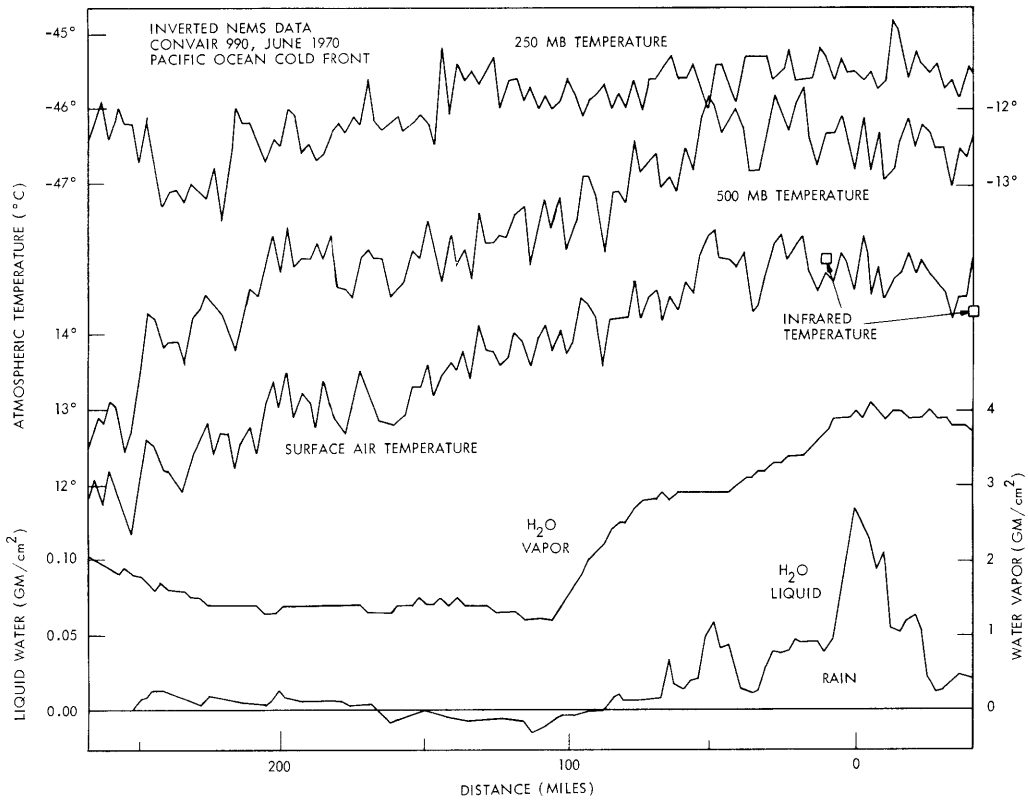

Fig. V-6. Inverted NEMS data, CONVAIR 990, June 1970. Pacific Ocean Cold Front.

For these reasons, the inversions for atmospheric temperature shown in Fig. V-6 make use of only the three oxygen band frequencies, 53.65, 54.90, and 58.80 GHz. Since the simultaneous estimation of vapor and liquid water makes use of the different spectral characteristics of the emission by the two phases, and the water-vapor emission is temperature-dependent, all five frequencies were used in the inversion for those two parameters.

P. W. Rosenkranz, D. H. Staelin

References

1. K. L. S. Gunn and T. W. R. East, Quart. J. Roy. Meteor. Soc. 80, 522 (1954).
2. C. H. Collie, D. M. Ritson, and J. B. Hasted, Proc. Phys. Soc. (London) 60, 145 (1948).
3. P. W. Rosenkranz, Quarterly Progress Report No. 99, Research Laboratory of Electronics, M.I.T., October 15, 1970, pp. 7-13.

C. OPTICAL STELLAR INTERFEROMETER

During the past quarter, construction of the optical stellar interferometer[1] has centered on the electronics associated with 12 photomultipliers that are to be used as detectors. Having decided that the signal processing for this experiment is to be entirely digital, we use the photomultipliers in the pulse-counting mode. As the counting rates will not be too high (<1 MHz), this is done by amplifying the anode signal with a Type 702 amplifier used with a gain of 100, followed by a Type 710 comparator used as a pulse-height discriminator and monostable multivibrator. The photomultiplier tubes are Type 4517.

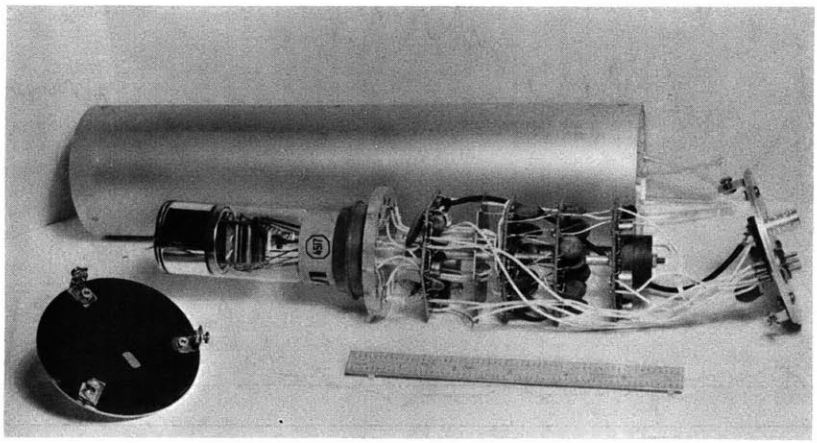

Fig. V-7. A photomultiplier tube and its associated circuitry.

Figure V-7 shows the arrangement of parts in one of the completed assemblies. The electronic parts are mounted on hexagonal etched boards that, from right to left, are an inverter and regulator, a diode multiplier chain to produce the 120 volts/stage used by the tube, a lowpass filter, an electrostatic shield, and the preamplifier assembly. In addition to the preamplifier and discriminator, the last assembly contains an emitter follower that drives the 50 Ω output cable, and a protective circuit that removes the voltage from the cathode when more than 3 μA flows in the 10^{th} dynode. These circuits are DC-coupled, and the tube is used with the cathode at -1400 V. The wire that extends beyond the front of the tube is used to connect the magnetic shield to cathode potential, thereby providing the required electrostatic shielding.

There are two reasons for using a separate high-voltage supply with each tube. First, the elimination of external high-voltage cabling should make the system more reliable under field conditions, where dew and other condensation might be a source of trouble. Second, the separate high-voltage supplies make the phototube assemblies

more versatile – to use them in other experiments, only readily available low voltages have to be supplied.

The outer shell of the assembly is 3" O.D. thin wall aluminum tubing. This is lined with styrofoam for thermal insulation, and the air tubes visible at the right end are used to control the temperature. The light enters through the hole in the front plate, which is off center to allow the sensitivity of the tube to be increased by multiple internal reflections inside the faceplate.

P. L. Kebabian

References

1. P. L. Kebabian and D. H. Staelin, "Long Baseline Stellar Interferometer," Quarterly Progress Report No. 90, Research Laboratory of Electronics, M.I.T., July 15, 1968, pp. 10-11.